Prediction of Mechanical Properties of TWIP Steels using Artificial Neural Network Modeling

M. M. Karkeh Abadi *[1] , A. Kermanpur [2], A. Najafizadeh [3], K. Kiani [4], S. Sabet[5]

[1, 2] Department of Materials Engineering, Isfahan University of Technology, Isfahan 84156-83111, Iran
[3] Foold Institute of Technology, Fouldshahar, Isfahan 8491663763, Iran
[4] Department of Computer Engineering, Semnan University, Semnan 35131-19111, Iran
[5] Department of Industrial Engineering, Semnan Branch of Islamic Azad University, Semnan 35135-179, Iran

Abstract

In recent years, great attention has been paid to the development of high manganese austenitic TWIP steels exhibiting high tensile strength and exceptional total elongation. Due to low stacking fault energy (SFE), cross slip becomes more difficult in these steels and mechanical twinning is then the favored deformation mode besides dislocation gliding. Chemical composition along with processing parameters has profound effects on SFE and mechanical properties of TWIP steels. In this work, artificial neural network (ANN) models were developed to predict tensile properties of these steels. In these models, %Mn, %Al, %Si, %C, cold rolling reduction, strain rate, annealing temperature, and time were chosen as input, while engineering yield strength (Y.S.), tensile strength (T.S.) and total elongation (T.E.) were considered to be output parameters. The network models were trained for each output individually. A reasonable agreement was found between the results of tensile tests and the predictions, showing the robustness of the present ANN models. The developed models can be used as a guide to achieve high strength and ductility by (i) alloy design or (ii) controlling processing parameters through the strain-induced twinning process.

Keywords: Artificial neural network; High manganese austenitic steel; TWIP steel; Mechanical properties; Stacking fault energy.

1. Introduction

There is an increasing demand to develop ultra-high strength steels (UHSSs), including dual phase, transformation induced plasticity (TRIP), twinning induced plasticity (TWIP) and boron steels in the auto steel industry [1)]. The motivations include reducing the weight of the cars, and consequently, increasing the fuel efficiency and reducing CO_2 emission combined with the preservation or improvement of its ductility for more complex car design and crash absorbing properties [2, 3)].

High-Mn steels (15–30 wt. % Mn) in either TRIP or TWIP illustrate large work hardening during plastic deformation owing to superior strength–ductility combination [3, 4)]. Both TRIP and TWIP steels have austenitic microstructure and low stacking fault energy (SFE). The austenite phase in both steels is usually stable under cooling, but not under mechanical load. Phase

* *Corresponding author*
Tel.: +98 912 3316943, Fax:+98 31 33912752
Email: mm.karkehabadi@gmail.com
Address: Department of Materials Engineering, Isfahan University of Technology, Isfahan, Iran
1. M.Sc.
2. Professor
3. Professor
4.Assistant Professor
5. M.Sc.

transformation occurs in TRIP steel under mechanical load; while in TWIP steels, mechanical twinning in austenite grains happens during cold deformation; even at high strain/strain rate levels [5, 6]. TWIP steels have a higher SFE than the TRIP ones. At very low SFE, the transformation of austenite (γ) to ε-martensite to α'-martensite occurs. At higher values, but less than ~20 mJ m^{-2}, the direct transformation of γ→ α' is preferred. For steels with SFE between 20 and 40 mJ m^{-2}, twinning is the main deformation mechanism [7, 8]. Although this austenite deformation mode is attributed to its SFE [9], generally, it is not a critical parameter, i.e. planar glide or wavy glide plays a pivotal role. In other words, the initiation of twinning requires a critical density of planar dislocations. The slip planarity in fcc alloys is mainly related to the following factors: (1) low SFE, (2) large lattice frictional stress, and (3) short-range ordering (SRO) [10].

Wide-extended partial dislocations in low SFE materials have the low three-dimensional mobility and therefore insufficient Burgers vector directions to form cells. Consequently, planar glide is favorable [11]. The SFE is affected by chemical composition, temperature and grain size [12, 13]. With an increase in Mn content, the SFE is first decreased to a minimum value and then it is increased (see Fig. 4 in [14]). Addition of Al raises the SFE so that the γ→ε transformation is strongly suppressed. In large quantities of Al, the TRIP or even TWIP could be prevented. Thus, dislocation slip may act as a favored mechanism of plastic deformation [8, 15]. Contrary to Al, experiments showed that Si decreases SFE and sustains the γ→ε transformation during cooling and deformation [16], while calculations concluded that the SFE is first peaked at 4 wt. % Si and then it is decreased (see Fig. 1 in [17]). Increasing the C content has a direct effect on SFE [18, 19]. Moreover, it is reported that SFE grows with temperature [12, 19, 20] or by decreasing the austenite grain size (especially below ~30 μm) in high Mn steels [21-23]. Nevertheless, some researchers have suggested that this SFE, called the "apparent SFE", is independent of grain size [13].

High Peierls-Nabarro (P-N) stress value and interaction among dislocations, twins, large additional atoms, and precipitates create large lattice frictional stresses, and then planar glide is favorable in work hardened high alloyed steels. Some researchers [11, 15] claimed that regardless of the value of the SFE in FCC alloys, 'Glide plane softening' phenomenon, attributed to SRO, is mainly responsible for planar glide. Passing the leading Shockley partial through the ordered lattice devastates the SRO, which is not able to restore itself because of its short range nature. Therefore, by activating a dislocation source, all other dislocations tend to slip on the same plane of leading partial gliding to minimize the imposed extra energy [10, 11, 15, 24]. This phenomenon is more preferential in the concentrated solid solutions alloys [11].

However, the research on TWIP steels is still in its beginning. According to the author's knowledge, limited works have been conducted on the prediction of mechanical properties of TWIP steels. There are some methods to predict materials properties [25-30], among which, ANN is a flexible structure, which has been broadly used especially when the underlying relationships between the inputs and outputs are unknown [31-37]. Dini et al.[9] predicted mechanical properties of TRIP/TWIP steels using the ANN modeling, but they only investigated the effect of chemical composition (as input) and neglected other manufacturing parameters. In the present work, in addition to chemical composition, some mechanical and heat treatment parameters were modeled by ANN for predicting tensile properties of TWIP steels. In addition, in all data taken from the literature, some effective conditions such as austenitic monophasic as-cast steel, achievement way to TWIP steel (combination of large cold rolling reduction and subsequently annealing treatment), tensile test temperature and no phase transformation after cold rolling, water quenching and tension were kept similar. Finally, by using the developed ANN models, the correlation between all the input and output variables will be plotted and analyzed and some probable dominant mechanisms operating on tensile properties will be discussed as well.

2. Methodology

2. 1. Network database

The required data for ANN models were taken from literature [3, 6, 15, 16, 21, 22, 24, 38-48] which comprises the chemical composition, cold rolling reduction, tension strain rate, annealing/solution treatment temperature and time as the input variables. Engineering Y.S., T.S., and T.E. were also taken as the output variables.

2. 2. Network architecture

In order to build reliable models, three substantial steps were taken. First, an individual network was designed for each output. As shown in Fig. 1, in each network, chemical compositions, mechanical and heat treatment parameters were reckoned as inputs. While, in the first network, Y.S., in the second one, T.S. and in the third one, T.E. were considered as outputs.

The second most important step was to determine the optimum number of hidden layers. Hornik [49] demonstrated one hidden layer by sigmoid (logarithm sigmoid or hyperbolic tangent) activation function can depict any function of practical issues. However, in the present study, one, two and three hidden layers were simulated. The highest correlation coefficients (R-value) between inputs and outputs data and the lowest mean squared error (MSE), which can be expressed below, were seen in ANN with two layers:

$$MSE=[1/N]\sum_{i=1}^{N}(y_i-t_i)^2 \quad \text{Eq. (1)}$$

, where t_i is the target and y_i is the network output.
Moreover, the third step was to determine the best neurons number in each layer. For this purpose, the Taguchi method was used. In this method, factors are divided into controllable and noise factors (on which there is no direct control). Using the concept of robustness in the Taguchi method minimizes the effect of noise, and determines the optimal level of controllable factors. For this purpose, Signal-to-Noise (S/N) ratio was defined. Where the term of signal denotes a desirable value (response variable) and noise stands for an undesirable value (standard deviation) [50]:

$$S/N=-10\log\left[1/n\sum_{i=1}^{n}\left(1/y_i^2\right)\right] \quad \text{Eq. (2)}$$

, where y_i is the response variable and n is the number of experiments.

In this work, two controllable factors, in which the first factor was related to the first layer and the second factor to the second one, were used. For each factor, four levels as representatives of the number of neurons were considered. Therefore, the combination of two sets of four levels introduced 16 various conditions. To determine the optimum condition by the Taguchi, four levels in each layer primarily started by 1, 2, 3 and 4 neurons. In parallel, ANNs are also used with two layers and 16 conditions, exactly like the Taguchi model. Then, the inferred MSE from ANNs is sent to the Taguchi model to calculate S/N ratio. When the highest mean S/N ratio is obtained at the terminal levels (see Fig. 2.), one will be added to previous neurons and the whole procedure is repeated by the new numbers. For instance, if the highest mean S/N ratio is gained at the 4th level of the first layer, this procedure will be run by 2, 3, 4 and 5 neurons for the levels of this layer. This process will persist until the highest mean S/N ratio is achieved in internal levels of both layers simultaneously.

2. 3. Activation function

As shown in Eqs. (3) and (4), the nonlinear radial basis and tansigmoid activation functions were used in the hidden layers, respectively, and purelin was employed at the output layer. The output of the radbas and tansig functions are in the range of (0, 1) and (-1,1), respectively.

$$y=\text{radbas}(x)=\exp(-x\text{^}2) \quad \text{Eq. (3)}$$

$$y=\text{tansig}(x)=[2/(1+\exp(-2x))]-1 \quad \text{Eq. (4)}$$

2. 4. Development of the ANN models

The gleaned data were divided randomly into three groups, 70% for the training set, 15% for the validation set and 15% for the testing set. The validation set is used to control the training process and the testing set is implementd to evaluate the generalization ability of the trained network. To improve the model performance, the input variables were normalized to bring the values between [0, 1].
Three supervised multilayered feed-forward topologies were employed in which units of each layer transfer their inputs received from the preceding layer's units to the units in the subsequent layer. In addition, the used algorithm was Levenberg-Marquardt. Since the ANN can be easily overtrained and can cause much larger error rate on new unseen data than the error rate on the training data, a stopping technique was applied in which the training process must be stopped and repeated when the measured error, using an independent validation set, starts to increase. After proper training, the models are able to relate the input to the output variables, and can subsequently predict the unknown outputs. This ability, which is called generalization, is assessed by testing sets.

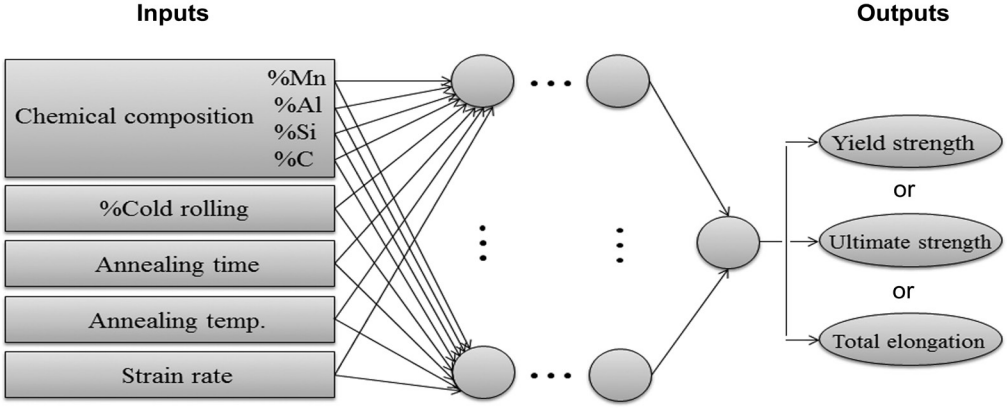

Fig. 1. Schematic representations of the ANNs employed for each output.

3. Results

As tabulated in Table 1, two controllable factors and four determined levels of Taguchi models can be seen. The performances of used ANNs for 16 conditions of levels were shown in Table 2, and their results, to determine optimum levels, were illustrated in Fig. 2. The highest value of mean S/N in Fig. 2 was selected as the optimum level. The optimum neurons and activation functions for ANN models are listed in Table 3 as well. The performance of training and generalization ability of each model was drawn in the scatter diagram for predicting values versus actual values, as can be seen in Fig. 3. Moreover, their R and the MSE values are presented in Table 4.

Using the developed models, surface maps were plotted for analyzing the correlation between chemical compositions, mechanical parameters, heat treatment parameters as input variables and tensile properties as the output variables. They were mapped in Figs. 4-7.

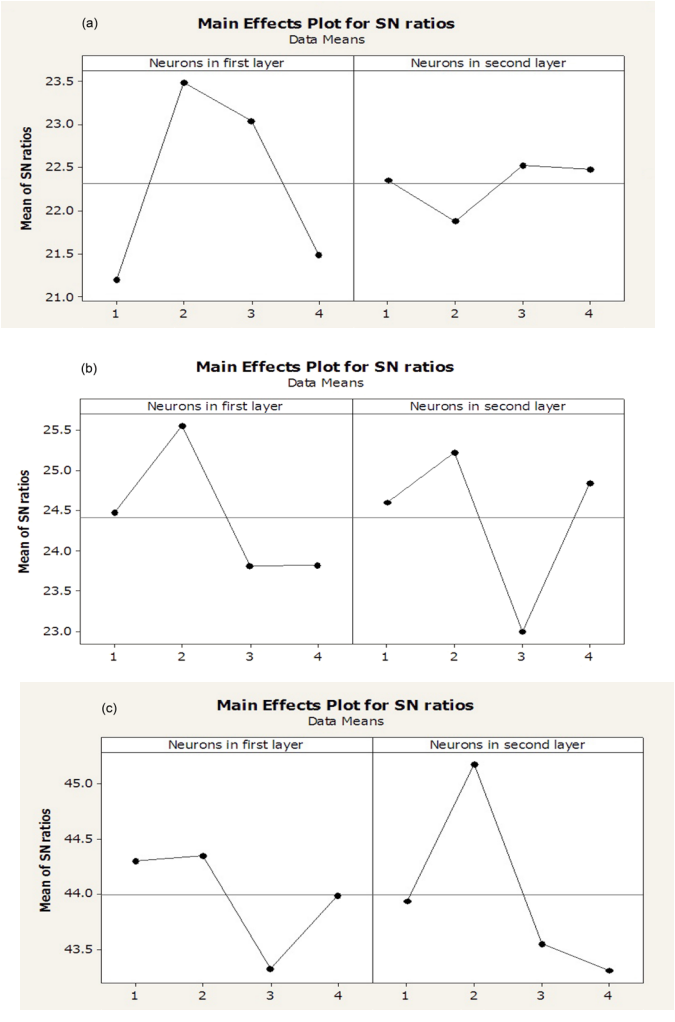

Fig. 2. Signal-to-Noise (S/N) ratio in Taguchi models

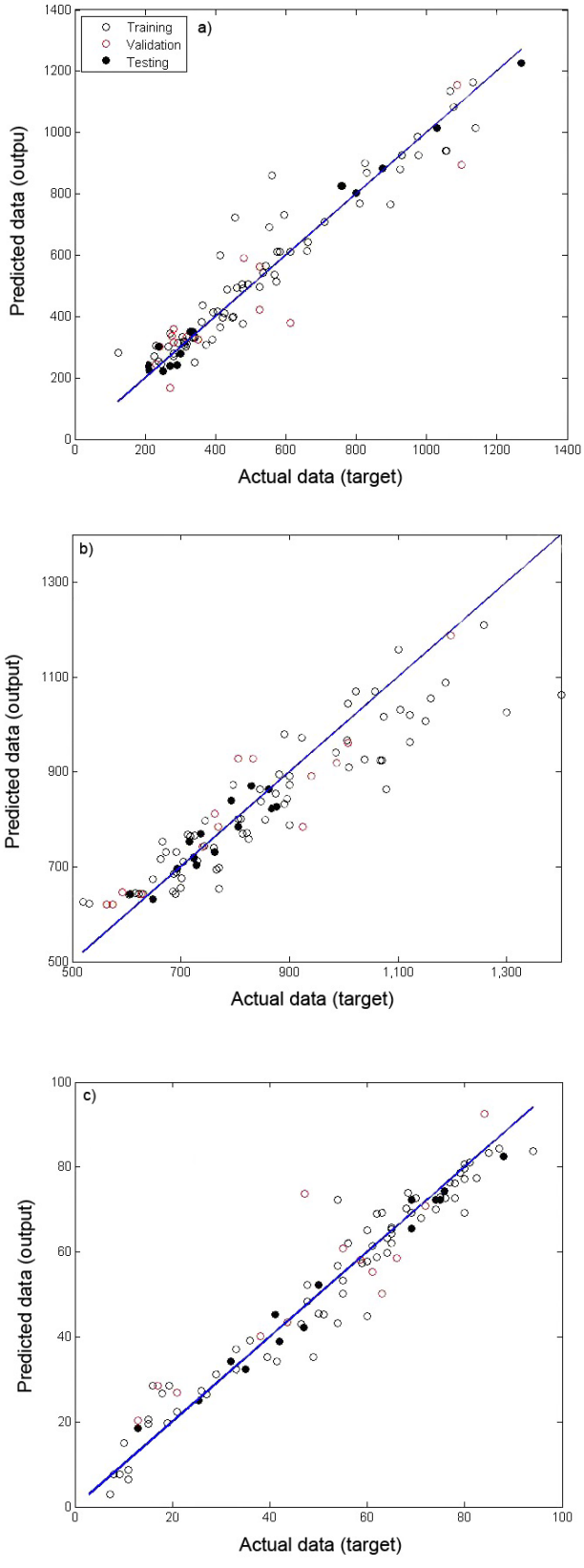

Fig. 3. Comparison between predicted (output) and actual values (target) for training, validation, and testing: a) Y.S., b) T.S., and c) T.E.

Table 1. Determined 4 levels for Taguchi models.

	Levels	1	2	3	4
Y.S.	No. of neurons at first layer	4	5	6	7
	No. of neurons at second layer	5	6	7	8
T.S.	No. of neurons at first layer	12	13	14	15
	No. of neurons at second layer	2	3	4	5
T.E.	No. of neurons at first layer	12	13	14	15
	No. of neurons at second layer	6	7	8	9

Table 2. The ANNs performance for 16 conditions of neurons, resulting from the combination of four levels of Taguchi models.

	No.	1	2	3	4	5	6	7	8	9	10	11	12	13	14	15	16
Y.S.	No. of neurons at first layer	4	4	4	4	5	5	5	5	6	6	6	6	7	7	7	7
	No. of neurons at second layer	5	6	7	8	5	6	7	8	5	6	7	8	5	6	7	8
	MSE	0.6446	0.11663	0.09246	0.08232	0.07731	0.07107	0.05186	0.05433	0.0835	0.08047	0.06735	0.0708	00.8115	0.06317	0.09706	0.101
T.S.	No. of neurons at first layer	12	12	12	12	13	13	13	13	14	14	14	14	15	15	15	15
	No. of neurons at second layer	2	3	4	5	2	3	4	5	2	3	4	5	2	3	4	5
	MSE	0.05316	0.05064	0.07746	0.06097	0.05267	0.0785	0.04305	0.0436	0.06179	0.06877	0.05919	0.06871	0.06933	0.05936	0.07002	0.05977
T.E.	No. of neurons at first layer	12	12	12	12	13	13	13	13	14	14	14	14	15	15	15	15
	No. of neurons at second layer	6	7	8	9	6	7	8	9	6	7	8	9	6	7	8	9
	MSE	0.00533	0.00585	0.0078	0.00568	0.00708	0.00384	0.00656	0.00757	0.00627	0.00681	0.00617	0.00818	0.00689	0.00605	0.00619	0.0062

Table 3. Conditions of the developed ANN models.

Neural network	Network architecture	Transfer functions
Y.S.	8-5-7-1	radbas-tansig-purelin
T.S.	8-13-3-1	radbas-tansig-purelin
T.E.	8-13-7-1	radbas-tansig-purelin

Table 4. The performance of the developed models for prediction of tensile properties of TWIP steels.

Neural network	Training		Validation		Testing	
	MSE	R-value	MSE	R-value	MSE	R-value
Y.S.	0.00608	0.95519	0.01097	0.92891	0.00124	0.99481
T.S.	0.00773	0.91627	0.00458	0.93073	0.00101	0.9169
T.E.	3.108exp-5	0.97265	9.269exp-5	0.89713	1.169exp-5	0.98985

4. Discussion

4. 1. Performance of the ANN models

Low values of MSE and relatively high R-values in Table 4 and Fig. 3 indicated the degree of accuracy of the developed models. It is important to recognize that although there were some effective factors limiting the precise predictive capability of the networks directly: (1) effect of grain size, (2) carbide precipitation, and (3) twins thickness and their spacing, determined inputs somehow; thus, compensating their effects indirectly.

Grain size affects the Y.S. according to the Hall-Petch relationship. Besides, twin boundaries, like grain boundaries, act as strong barriers to the subsequent movement of dislocations [8]. They provide decrease in the dislocation mean free path, causing the strength of the materials to be increased (the so-called dynamic Hall–Petch effect) [51]. Therefore, the strengthening mechanisms during deformation include both typical work hardening due to the restricted dynamic recovery in these low SFE steels and a second hardening attributed to the mechanical twinning [21, 22, 39].

Carbide precipitation can also improve the strength properties. In the equilibrium phase diagrams of Fe–Mn–Al–C alloys, there are two types of carbides including M_3C ($(Fe,Mn)_3C$) and κ ($(Fe,Mn)_3AlC$) in the high-temperature region, which are stable even at room temperature. In high Mn alloys with low or without Al content, M_3C carbides are more important than the κ carbides, which can form in high Al (more than 5%) and high C (more than 1%) alloys [38]. Both carbides precipitation reduce the amount of carbon in austenite, thereby SFE of the steel is decreased [52].

As mentioned before, dislocation/carbon interactions promote the planarity of slip. Dislocation pile-ups can raise local stress concentrations and provide more potential sites for twin nucleation, but these interactions suppress twin growth and hence result in the formation of thinner and denser twins lamellae and twin bundles [47].

4. 2. Applications of the ANN models

Based on what was mentioned, all specimens are deformed in two stages: (1) cold rolling and (2) tensile tests. Since no phase transformation occurred after cold rolling and tension, competition between the occurrence of mechanical twinning and dislocation slip is important during the evaluation of input factors affecting the tensile test results. In should be noted that the plots for each pair of input variables (for instance Mn-Al) were depicted when the other input variables (%Si, %C, %reduction, strain rate, annealing time, and temp.) were constant.

4. 2. 1. Effect of chemical composition

a) Mn and Al:

As shown in Fig. 4a, the Y.S. decreased with an increase in the Mn or Al contents. Due to the increase in SFE by adding the Mn or Al contents, slip can become the predominant mechanism during cold rolling and the tensile test, which tends to lower the density of mechanical twinning. This reduction results in a descent in the Y.S., as was expected based on the results of another report [53] for two reasons: (1) a higher percentage of the appropriate crystallographic directions for dislocation slip and (2) decrement of dynamic Hall–Petch effect that leads to an increase in dislocation movement space.

Moreover, Al is a graphite stabilizer; therefore, it slows down the carbide precipitation. Hence, carbide precipitation is not high enough to reduce the amount of carbon in austenite and decreases its SFE. As can be seen, solid solution strengthening mechanism by adding Al is not effective for improving the Y.S. in TWIP steel [16, 54].

In Fig. 4b, the T.S. dropped with an increase in the Mn or Al contents, as already confirmed by other investigations [1, 16, 48, 53, 55]. The change by Al was more significant than Mn. Mn or Al content as SFE raiser provides low density of mechanical twinning, and as a consequence, the T.S. decreases. Al addition increases the thickness of deformation twinning and results in a decrease in the interfaces between deformation twins and the γ matrix; therefore, work-hardening ability will be reduced [54]. Besides, Al reduces dynamic strain aging (DSA) because of reductions in both activity and diffusivity of C in austenite [16, 56]. The certain increased T.S. in high Mn-Al alloys can be attributed to the formation of κ carbides from one side and SFE decrement by carbide precipitation from another side.

In TWIP steels, the strain-induced deformation twins, similar to martensitic phases in TRIP steels, preferentially take place in γ matrix in the area where local necking tends to occur (TRIP effect). In this local deformation region, dislocation motion will be retarded (dynamic Hall–Petch effect) and the local strength of the material is surged due to the intensive local strain hardening. Surrounding areas will deform to achieve the strength. Thus, the uniform elongation can be enhanced [3-5, 9, 55]. As shown in Fig. 4c, the T.E. raised by Mn or Al contents and decreased in alloys with high amounts of Al and Mn. High SFE of alloys and therefore descent in TWIP effect, and presence of preferential nucleation sites for crack initiation on interfaces between hard carbides and the austenite can be the reasons.

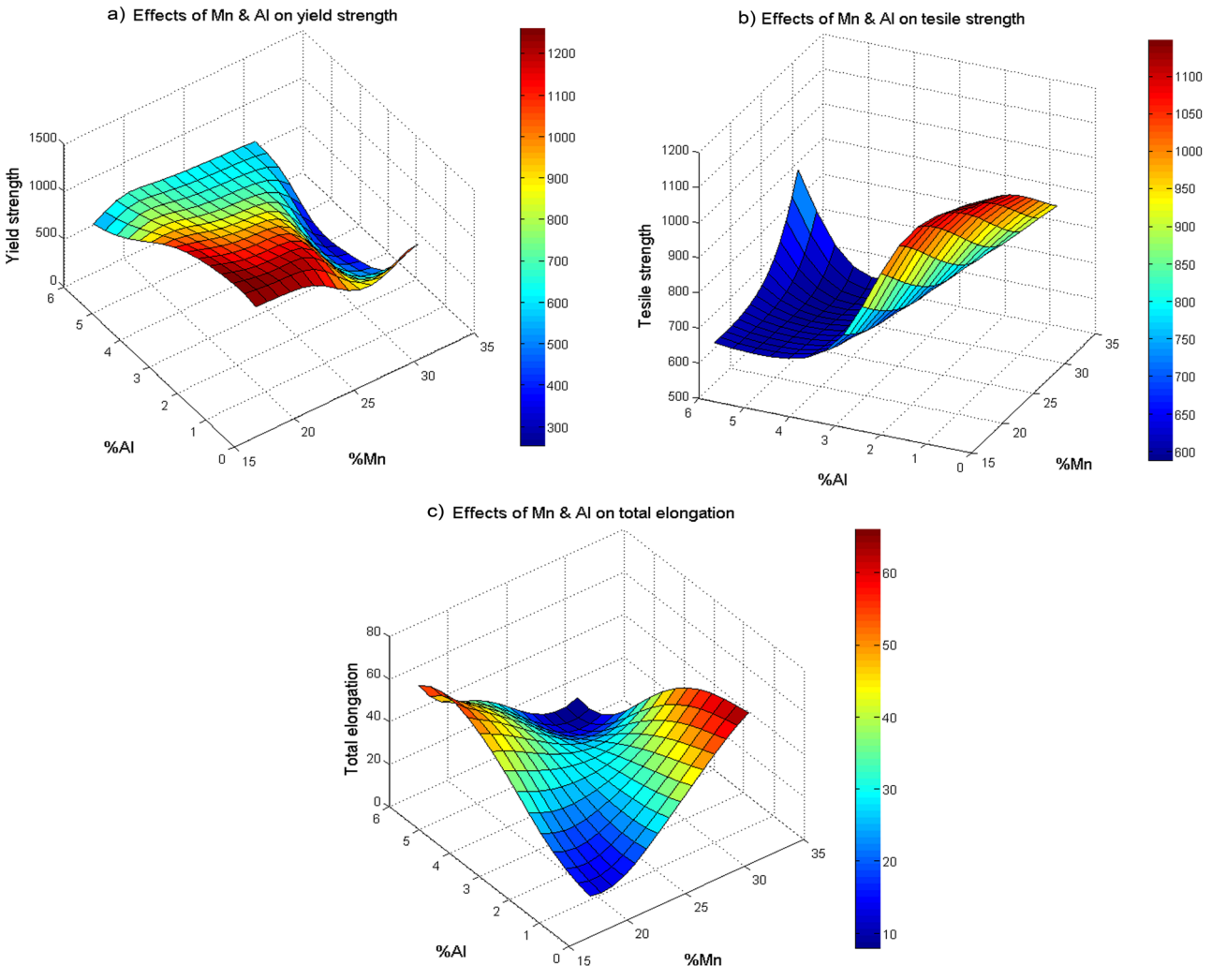

Fig. 4. The surface plot for a) Y.S. b) T.S. and c) T.E. as a function of %Mn & %Al.

b) Si and C:

As presented in Fig. 5a, the Y.S. increased with an increase in the Si or C contents. Although Si, like Al, is a graphite stabilizer and prevents carbide formation, it can lead to the increase in Y.S. by solid solution strengthening, grain refinement 16) and the twinning mechanism by decreasing SFE. Generally, increasing C content influences the Y.S. due to the following remarks: (1) solid solution strengthening, (2) increasing the probability of dislocation/carbon interactions and promotion to finer twins lamellae, (3) increasing the probability of carbide formation, and (4) dipping the probability of twinning occurrence owing to the increased SFE. Here, the first three items are more predominate.

The increased ultimate T.S. by increasing the Si or C contents is shown in Fig. 5b. In spite of decrement of carbide formation and the C diffusivity (and DSA), the T.S. increased due to SFE decrease, originating from Si content and also significant strain hardening by secondary mechanical twins. Si rapidly increases the volume fraction of the secondary mechanical twins [16]. Improved strain hardening capacity by increasing the C content due to the strong atomic interaction of C with dislocations and twins (DSA), possible carbide formation, the formation of thinner and denser twins and twin bundles overshadowed the SFE enhancement, thereby increasing the T.S..

Figs. 5a and b illustrated that the effect of C on the Y.S. was more remarkable than T.S.. In the high alloyed steels with Si and C, SFE decrement by Si was compensated by C addition and the Y.S. and T.S. were partially declined, in comparison to high Si ones.

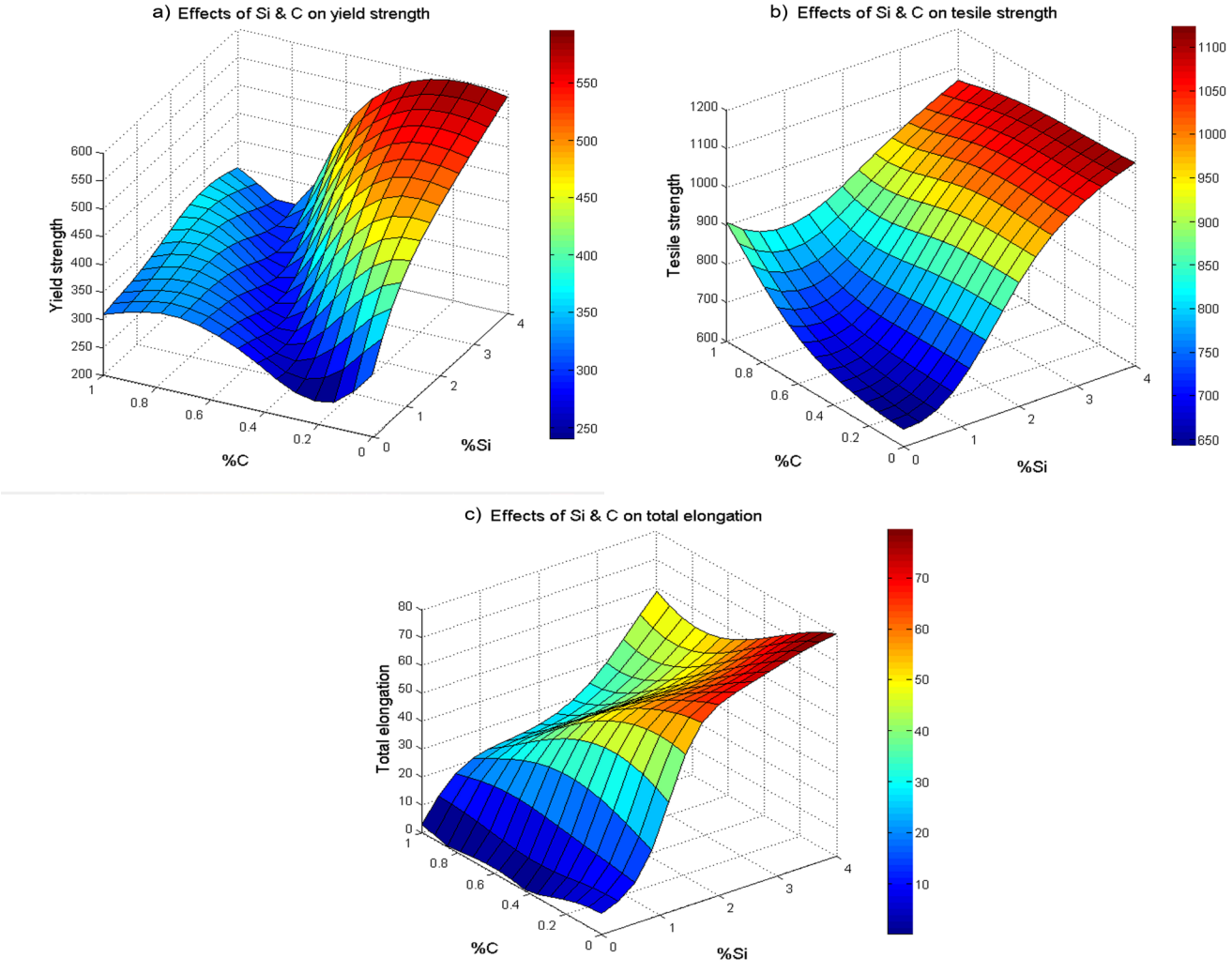

Fig. 5. The surface plot for a) Y.S. b) T.S. and c) T.E. as a function of %Si & %C.

In Fig. 5c, T.E. values exhibit a dramatically upward trend by Si and a gradual downward trend by C. The increased secondary mechanical twins by Si raised the T.E.. Increasing C content decreases TWIP effect during two stages of deformations by SFE enhancement. Moreover, the interfaces between hard carbides and the matrix act as preferential nucleation sites for crack initiation.

4. 2. 2. Effect of deformation parameters

As shown in Figs. 6a and b, the Y.S. and the T.S. increased with cold rolling and increased or remained constant via strain rate, which is in good agreement with other reports [3, 4, 6, 8]. The volume fraction of nano-scale mechanical twins grew with increasing strain. Even several twinning systems may also be activated in some areas 23). Meanwhile, in low SFE metals such as TWIP steel, dynamic recovery is restricted. Thereby, because of the presence of mechanical twins and dynamic Hall–Petch effect, the Y.S. is increased.

Several phenomena including (1) adiabatic heating [3, 7, 8], (2) decrease in the average time of dislocation piling up at obstacles [54], and (3) extensive formation of twins [7] may occur at high strain rate. The adiabatic heating of the sample during the tensile test leads to the SFE enhancement, causing the decrement in the fraction of twinned grains and concurrently enhancement in the thickness of deformation twins [54], or even replacement of twinning with dislocation slip. Adiabatic heating and decreased piling up time are balanced with the formed extensive twins at the first stage of reduction, while the latter overcomes slightly above 55%.

In Fig. 6c, the T.E. increased and then droped by strain. TRIP effect and several twinning systems caused high-value elongations at low to medium degree of reduction. At high deformation, grain boundaries, the intersection of non-parallel twin systems and twin-grain boundary interfaces or places where a twin reaches a free surface are preferential nucleation sites for cracking [57, 58] (see

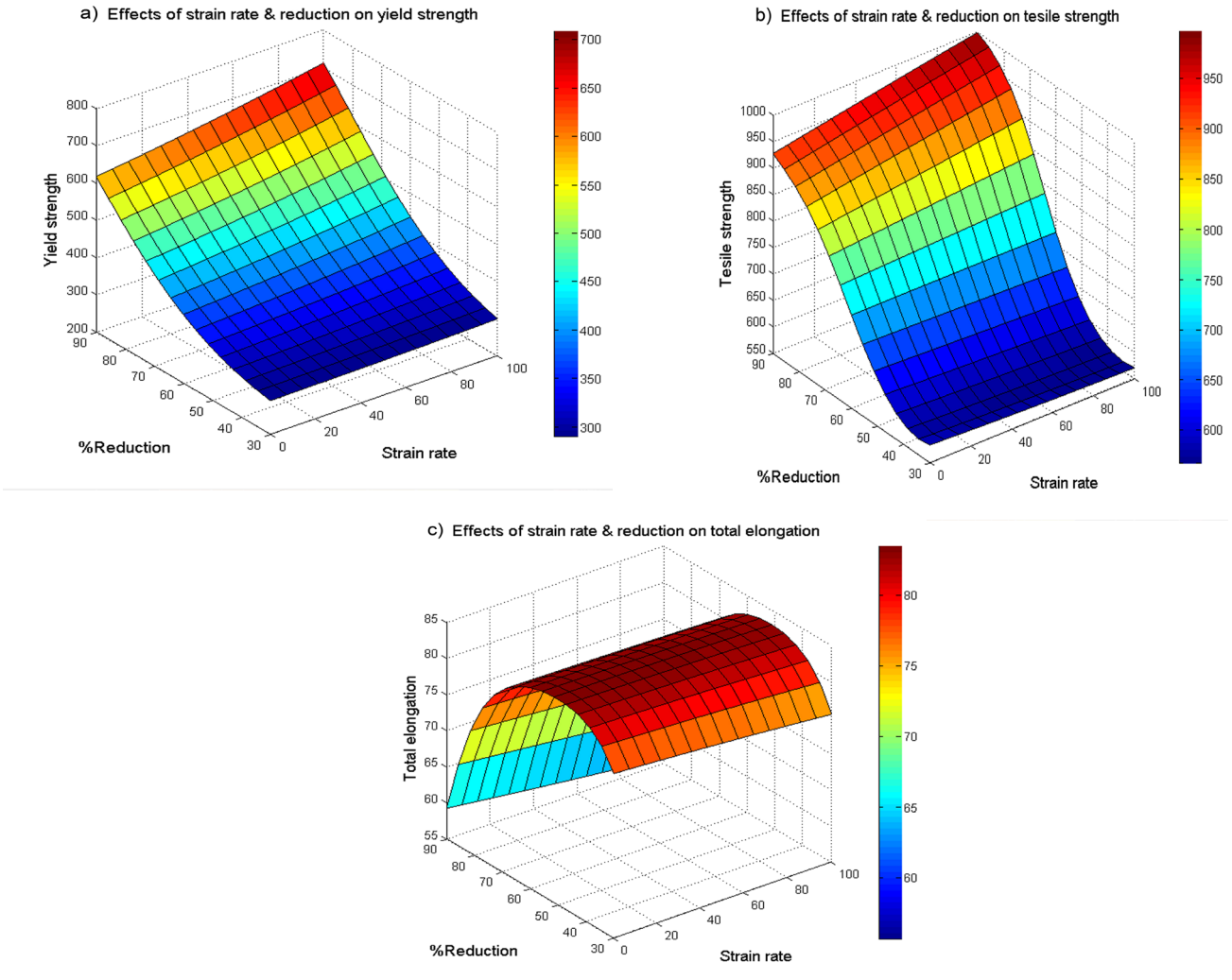

Fig. 6. The surface plot for a) Y.S. b) T.S. and c) T.E. as a function of strain rate & %reduction.

Fig. 5 in [57]). In addition, around a twin, prevented from further growth by a barrier twin, the highest stresses will develop and the resultant pile-up produces a very high static stress field that causes cracking [58]. Formation of microvoids because of disintegrated inclusion with matrix under deformation is another origin of failure (see Fig. 4 in [57]).

After achieving a relative maximum strain rate, the uniform elongation decreased [4, 8, 54] slightly. Descent in the elongation values is ascribed to the produced adiabatic heating of the specimen during the tensile test. It makes twin thicker and sparser and displacement of dislocation slip instead of twinning.

4. 2. 3. Effect of annealing parameters

The Y.S. and the T.S. fell with increasing the annealing time/ temperature, as can be seen in Figs. 7a and b. They dropped rapidly in the range of 550-750 °C. As expected, the annealing temperature was more effective than time. Konopka et al. [59] reported that increasing the frequency of annealing twin boundaries causes a reduction in the Y.S.. This reduction is attributed to the activation of dislocation sources on twin boundaries (see Fig. 3 in [59]). In this circumstance, the twin boundary undermines the strength of the material. On the other hand, Behjati and Asgari [10] reported that annealing twin boundaries, like mechanical twin boundaries, acts as cross slip obstacles as well (see Fig. 3 in [10]). Grain growth during annealing, an annihilation of mechanical twinning/dislocation and therefore decrease in dynamic Hall–Petch effect, and annealing twin boundaries as the Frank-Reed source situations are the probable predominant factors in the Y.S. and the T.S. decrement.

As shown in Fig. 7c, the T.E. raised by the annealing time/ temperature because of grain growth and activation of dislocation generation sources. Although change in T.E. by time was visible, it could be neglected versus the effect of temperature.

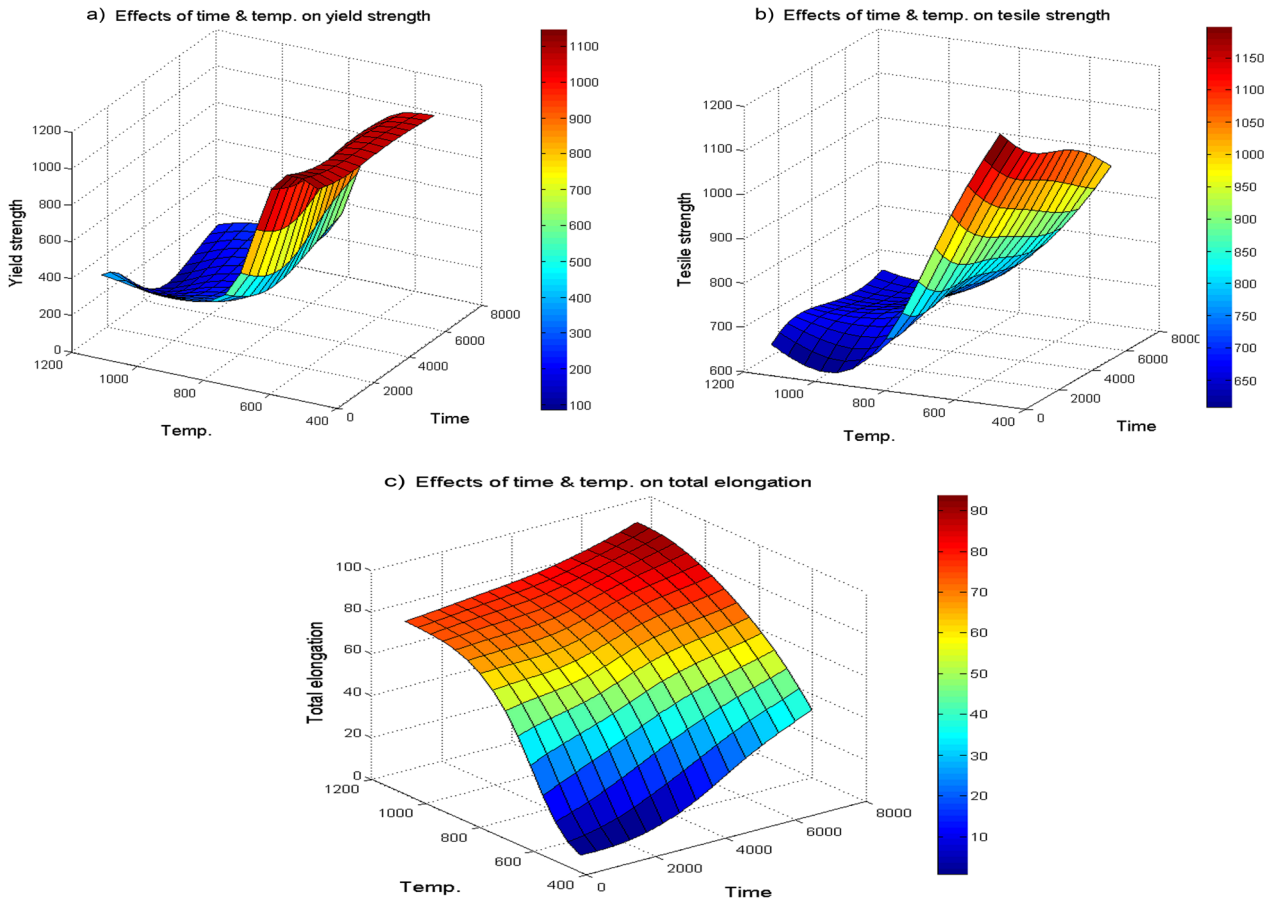

Fig. 7. The surface plot for a) Y.S. b) T.S. and c) T.E. as a function of annealing time & annealing temperature.

5. Conclusions

- The best correlation was found for the ANN models by one single output instead of multiple outputs.
- The Y.S. and the T.S. dropped with an increase in the Mn or Al contents. In TWIP steels, solid solution strengthening mechanism by Al addition is not effective to improve the Y.S.. Moreover, change in the T.S. by Al was more significant than Mn. The T.E. increased with an increase in the Mn or Al contents and decreased in high alloys with Al and Mn amounts. The reasons can be a decrease in TWIP effect and the presence of preferential nucleation sites for crack initiation on interfaces between hard carbides and the austenite.
- Increasing the Si or C contents leads to an increase in the Y.S. and T.S.; but in the high alloyed steels with Si and C, SFE decrement by Si was compensated by C addition and the Y.S. and T.S. were decreased. The effect of C on the Y.S. was more remarkable than T.S.. The T.E. values surged by Si and fell gently by C.
- The Y.S. and the T.S. were independent of strain rate before 55% reduction, and afterwards, they were increased modestly and directly. However, overall, the cold rolling reduction was more effective than the strain rate on Y.S., T.S., and T.E.
- The Y.S. and T.S. fell rapidly by increasing the annealing temperature, which was drastic in the range of 550-750°C. The annealing time was not so effective on Y.S, T.S, and T.E compared to the temperature.
- The appropriate range of chemical compositions and processing parameters for superior strength-ductility through the strain-induced twinning process was determined based on ANN models.

References

[1] Z. L. Mi, D. Tang, L. Yan and J. Guo: J. Mater. Sci. Technol., 21(2005), 451.
[2] S. Vercammen, B. Blanpain, B.C. De Cooman and P. Wollants: Acta Mater., 52(2004), 2005.
[3] O. Grässel, L. Kruger, G. Frommeyer and L.W. Meyer: Int. J. Plast., 16(2000), 1391.
[4] R. Xiong, R. Fu, Y. Su, Q. Li, X. Wei and L. Li: J. Iron Steel Res. Int., 16(2009), 81.
[5] Z. L. Mi, D. Tang, H. Jiang, Y.J. Dai and S.S. Li: Int. J. Miner. Metall. Mater., 16(2009), 154.

[6] R. Ueji, K. Harada, A. Takemura and K. K.: Mater. Sci. Forum., 584-586 (2008), 673.
[7] S. Curtze and V.T. Kuokkala: Acta Mater., 58(2010), 5129.
[8] J. Yoo, S. Hwang and K.T. Park: Mater. Sci. Eng., 508(2009), 234.
[9] G. Dini, A. Najafizadeh, S. M. Monir-Vaghefi and A. Ebnonnasir: Comput. Mater. Sci., 45(2009), 959.
[10] P. Behjati and S. Asgari: Mater. Sci. Tech., 27(2011), 1858.
[11] J. D. Yoo and K. T. Park: Mater. Sci. Eng., 496(2008), 417.
[12] B. X. Huang, X. D. Wang, Y. H. Rong, L. Wang and L. Jin: Mater. Sci. Eng., 438-440(2006), 306.
[13] G. Dini, A. Najafizadeh, S. M. Monir-Vaghefi and R. Ueji: J. Mater. Sci. Tech., 26(2010), 181.
[14] A. S. Hamada: University of Oulu, Finland, (2007).
[15] K. T. Park, K. Jin, S. Han, S. Hwang, K. Choi and C. S. Lee: Mater. Sci. Eng., 527(2010), 3651.
[16] K. Jeong, J. E. Jin, Y.S. Jung, S. Kang and Y.K. Lee: Acta Mater. ,61(2013), 3399.
[17] A. Dumay, J.P. Chateau, S. Allain, S. Migot and O. Bouaziz: Mater. Sci. Eng., (2008), 184.
[18] X. Wang, H.S. Zurob, J.D. Embury, X. Ren and I. Yakubtsov: Mater. Sci. Eng., 527(2010), 3785.
[19] S. Allain, J.P. Chateau, O. Bouaziz, S. Migot and N. Guelton: Mater. Sci. Eng., 387-389(2004), 158.
[20] A.S. Hamada, L.P. Karjalainen and M.C. Somani: Mater. Sci. Eng., 467(2007), 114.
[21] R. Ueji, N. Tsuchida, D. Terada, N. Tsuji, Y. Tanaka, A. Takemura and K. Kunishige: Scripta. Mater., 59(2008), 963.
[22] G. Dini, A. Najafizadeh, R. Ueji and S.M. Monir-Vaghefi: Mater. Des., 31(2010), 3395.
[23] I. Gutierrez-Urrutia, S. Zaefferer and D. Raabe: Mater. Sci. Eng., 527(2010), 3552.
[24] C. Haase, L.A. Barrales-Mora, F. Roters, D.A. Molodov and G. Gottstein: Acta Mater. , 80(2014), 327.
[25] D.W. MacLachlan and D. M. Knowles: Mater. Sci. Eng., 302(2001), 275.
[26] P. D. Hoddson and R.K. Gibbs: ISIJ Int., 32(1992), 1329.
[27] Q. Zhang and M. Mahfouf: Appl. Soft Comput. , 11(2011), 2419.
[28] E. Zalnezhad, A. A. D. Sarhan and M. Hamdi: Int. J. Adv. Manuf. Tech., 68(2013), 415.
[29] Q. Hanchenga, X. Bocai, L. Shangzheng and W. Fagen: J. Mater. Process Tech., 122 (2002), 196.
[30] L. Gusel, R. Rudolf and M. Brezocnik: Int. J. simul. model., 14(2015), 39.
[31] H. Mirzadeh and A. Najafizadeh: Mater. Charact., 59(2008), 1650.
[32] H. Mirzadeh and A. Najafizadeh: J. Alloys Compd., 476(2009), 352.
[33] H. Mirzadeh and A. Najafizadeh: Mater. Des., 30(2009), 570.
[34] S.M.K. Hosseini, A. Zarei-Hanzaki, M. J. Yazdan Panah and S. Yue: Mater. Sci. Eng., 374(2004), 122.
[35] Z. Guo and W. Sha: Comput. Mater. Sci., 29 (2004), 12.
[36] S. Mandal, P. V. Sivaprasad, S. Venugopal, K. P. N. Murthy and R. Raj: Mater. Sci. Eng., 85 (2008), 571.
[37] T. Bhattacharyya, S.B. Singh, S. Sikdar (Dey), S. Bhattacharyya, W. Bleck and D. Bhattacharjee: Mater. Sci. Eng., 565(2013), 148.
[38] S. Kang, Y. Jung, J. Jun and Y. K. Lee: Mater. Sci. Eng., 527(2010), 745.
[39] G. Dini, A. Najafizadeh, R. Ueji and S. M. Monir-Vaghefi: Mater. Lett., 64(2010), 15.
[40] T. S. Shun, C.M. Wan and J. G. Byrne: Acta Metall. Mater., 40(1992), 3407.
[41] T. S. Shun, C.M. Wan and J. G. Byrne: Scripta. Metall. Mater., 25(1991), 1769.
[42] K. H. So, J. S. Kim, Y. S. Chun, K. T. Park, Y. K. Lee and C. S. Lee: ISIJ Int., 49(2009), 1952.
[43] M. O. Spindola, E.A.S. Ribeiro, B. M. Gonzalez and D. B. Santos: Revista Matéria, 15(2010), 143.
[44] L. Dazhao, W. Yinghui, S. Jinlu and H. Lifeng: Journal of Wuhan University of Technology-Mater. Sci. Ed. , 30(2015), 386.
[45] K. Wang, D. Wang and H. Han: Acta Mech. Sin., (2015), 1.
[46] S. Kang, J.G. Jung, M. Kang, W. Woo and Y.K. Lee: Mater. Sci. Eng., 652(2016), 212.
[47] S. Liu, L. Qian, J. Meng, P. Ma and F. Zhang: Mater. Sci. Eng., 639(2015), 425.
[48] O. Grässel, G. Frommeyer, C. Derder and H. Hofmann: J. Phys. IV., (1997), 383.
[49] K. Hornik, M. Stinchcombe and H. White: Neural Net., 2(1989), 359.
[50] N. K. Sharma and E. A. Cudney: Int. J. Eng. Sci. Tech., 3(2011), 15.
[51] O. Bouaziz, S. Allain and C. Scott: Scripta. Mater., 58(2008), 484.
[52] M. Iker, D. Gaude-Fugarolasb, P.J. Jacques and F. Delannay: Adv. Mater. Res., 15-17(2007), 852.
[53] C.Y. Chao and C. H. Liu: Mater. Trans., 43(2002), 2635.
[54] H. K. Yang, Z. J. Zhang, F. Y. Dong, Q.Q. Duan and Z.F. Zhang: Mater. Sci. Eng., 607(2014), 551.
[55] H. Ding, Z.Y. Tang, W. Li, M. Wang and D. Song: J. Iron Steel Res. Int., 13(2006), 66.
[56] J. E. Jin and Y.K. Lee: Acta Materia. , 60(2012), 1680.
[57] Z. L. Mi, D. Tang, Y.J. Dai, H.T. Jiang and J.C. Lü: Int. J. Miner. Metall. Mater., 16(2009), 646.
[58] J.w. Christian and S. Mahajan: Prog. Mater. Sci., 39(1995), 131.
[59] K. Konopka, J. Mizera and J.W. Wyrzykowski: J. Mater. Process. Tech., 99(2000), 255.